THE JOURNAL OF PHYSICAL CHEMISTRY B

pubs.acs.org/JPCB Article

Coumarin Partitioning in Model Biological Membranes: Limitations of log *P* as a Predictor

Katelyn M. Duncan, Aoife Casey, Christine A. Gobrogge, Rhys C. Trousdale, Stefan M. Piontek, Matthew J. Cook, William H. Steel, and Robert A. Walker*

Cite This: *J. Phys. Chem. B* 2020, 124, 8299–8308 Read Online

ACCESS | Metrics & More | Article Recommendations | Supporting Information

ABSTRACT: Time-resolved fluorescence measurements were used to quantify partitioning of three different 7-aminocoumarin derivatives into DPPC vesicle bilayers as a function of temperature. The coumarin derivatives were structurally equivalent except for the degree of substitution at the 7-amine position. Calculated log *P* (octanol: water partitioning) coefficients, a common indicator that correlates with bioconcentration, predict that the primary amine (coumarin 151 or C151) would experience a ∼40-fold partition enrichment in polar organic environments ($\log P_{C151}$ = 1.6) while the tertiary amine's (coumarin 152 or C152) concentration should be >500 times enhanced ($\log P_{C152}$ = 2.7). Both values predict that partitioning into lipid membranes is energetically favorable. Time-resolved emission spectra from C151 in solutions containing DPPC vesicles showed that within detection limits, the solute remained in the aqueous buffer regardless of temperature and vesicle bilayer phase. C152 displayed a sharp uptake into DPPC bilayers as the temperature approached DPPC's gel−liquid crystalline transition temperature, consistent with previously reported results ([*J. Phys. Chem. B* **2017**, *121*, 4061−4070]). The secondary amine, synthesized specifically for these studies and dubbed C151.5 with a measured log *P* value of 1.9, partitioned into the bilayer's polar head group with no pronounced temperature dependence. These experiments illustrate the limitations of using a gross descriptor of preferential solvation to describe solute partitioning into complex, heterogeneous systems having nanometer-scale dimensions. From a broader perspective, results presented in this work illustrate the need for more chemically informed tools for predicting a solute tendency for where and how much it will bioconcentrate within a biological membrane.

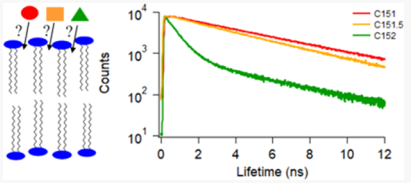

INTRODUCTION

Solute affinity for biological membranes is an extensively studied topic, given the importance of membrane partitioning in pharmaceutical applications and environmental toxicology.[1−6] The ability for solutes to partition into nonpolar phases underpins the general phenomenon of bioaccumulation as the basis for regulatory limits, used to identify harmful levels of pollutants in natural and municipal water systems.[7−10] While certain methods can be used to identify solutes that are likely to partition more readily into membranes, most bioaccumulation predictors are based either upon empirical results or models that simply use properties such as functional group additivity and overall solute polarity.[7,11] Missing are considerations of how subtle structural changes can affect a solute's affinity for one solvation environment over another.[12]

Solute uptake into biological organisms is often reported using either bioaccumulation or bioconcentration factors, with the difference being in the source of solute exposure.[10] Bioaccumulation is defined as an organism's uptake of a solute from any environmental source, including dietary uptake, inhalation, metabolic transformation, dilution through organism growth, and excretion.[10] Bioaccumulation is often characterized by the bioaccumulation factor (BAF), which reports the ratio of the solute concentration in the organism (C_B) relative to the sum of the solute concentrations in sediment (C_S), water (C_W), and food (C_F) (eq 1).

$$\mathrm{BAF} = \frac{C_B}{C_S + C_W + C_F} \quad (1)$$

The bioconcentration factor (BCF) is the most common measure of solute partitioning and refers to the solute absorption through respiratory and dermal surfaces alone. Diet is not included. The BCF is defined as the ratio of the concentration of the solute within the organism to the concentration of the solute in the water (eq 2).[10,13]

$$\mathrm{BCF} = \frac{C_B}{C_W} \quad (2)$$

The BAF and BCF are commonly used to describe a solute's persistence in the environment, but they can be difficult to measure directly. One empirical tool often used to predict a

Received: July 3, 2020
Revised: August 19, 2020
Published: August 25, 2020

https://dx.doi.org/10.1021/acs.jpcb.0c06109
J. Phys. Chem. B 2020, 124, 8299–8308

solute's tendency to bioconcentrate in membranes is the octanol–water coefficient (log *P*) (eq 3).[10,14,15]

$$\log P = \log\left(\frac{[\text{solute}]_{\text{octanol}}}{[\text{solute}]_{\text{water}}}\right) \quad (3)$$

The log *P* scale has a long and distinguished history and was first developed to better understand the intermolecular forces between synthetic organics and biomacromolecules.[16] Prior to the 1970s, scientists and pharmacologists used the log *P* scale as the primary standard to predict narcotic uptake and drug activity to screen solute bioavailability.[3,5] Subsequently, high-throughput screening (HTS) techniques have been developed, allowing solutes to be targeted and selected based on the log *P* values of analogs. HTS provided the ability to screen several compounds quickly; however, the resulting solute libraries required additional filtering to assess chemical functionality. Thus, HTS techniques started to shift the balance from simple solute solubility considerations to a more molecular perspective based on chemical functionality to account for solute–solute and solute–target interactions.[2,5,6,12,16,17]

In the l990s, Lipinski et al. proposed a set of criteria for evaluating solute affinity for absorption, distribution, metabolism, and excretion (ADME) that is now referred to as the Lipinski Rule of Five (Ro5).[2,17] The Ro5 considers certain molecular properties intended to capture solutes that display effective ADME behavior. Solutes likely to bioconcentrate will have (1) molecular weight less than 500 g/mol; (2) a calculated log *P* greater than 0 but less than 5.0; (3) 5 or less H-bond donors; and (4) fewer than 10 H-bond acceptors.[5,17] Solutes with some and/or all of these properties, including candidate pharmaceuticals, are predicted to have the right balance of hydrophilic and hydrophobic properties allowing for solubility in the bloodstream and the ability to partition into the organic interior of membranes. Interestingly, three of the four criteria of the Ro5 are that criteria depend simply on solute structure (molecular weight, hydrogen bond acceptors, hydrogen bond donors). Only the log *P* criterion requires experimental measurement; however, log *P* can also be calculated using computational tools that combine the additive partitioning characteristics of a solute's individual functional groups.[14,18,18–20]

The experiments described in this work examine how small changes in solute structure affect a solute's tendency to partition into model biological membranes. Moreover, our results also identify where in the membrane solutes accumulate. This work extends the scope of previous studies that quantified the partitioning a 7-aminocoumarin, Coumarin 152 (or C152, 7-dimethylamino-4-(trifluoromethyl)chromen-2-one) into lipid vesicle bilayers.[21–24] Specifically, the results presented below illustrate how small changes in solute structure can induce large changes in solute partitioning into biological membranes. Furthermore, the small differences in molecular architecture can create a large difference in the partitioning behavior which is not captured using a log *P* model. The three solutes used in this study are all 7-amino-4-(trifluoromethyl)chromen-2-one Coumarin derivatives, and they vary solely in their substitution at the 7-amino position. C152 is a tertiary amine that can only accept hydrogen bonds, whereas Coumarin 151 (C151: 7-amino-4-(trifluoromethyl)-chromen-2-one) is a primary amine capable of both accepting and donating hydrogen bonds. Both are commercially available. The corresponding secondary amine is not commercially available and was synthesized for these studies. For convenience, this solute was dubbed Coumarin "151.5" (C151.5: 7-methylamino-4-(trifluoromethyl)chromen-2-one). In the studies described below, the Coumarin derivatives are identified collectively as "C15X" (Figure 1).

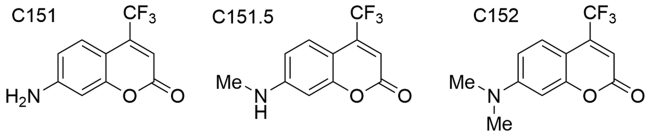

Figure 1. Coumarin derivative structures from left to right: C151, C151.5, and C152.

Log P coefficients for C151, C151.5, and C152 were calculated using ChemDraw Prime 19.0. These coefficients scale with increasing hydrophobic content—1.6 (C151), 1.9 (C151.5), and 2.7 (C152)—but all three values meet the Lipinski Ro5 log *P* criterion. It is worth noting the variability in log *P* values depends on how they are calculated and/or measured.[25,26] The molecular weight and hydrogen bonding opportunities also fall within acceptable Ro5 limits, implying that each solute should show a strong affinity for biological membranes in comparison to water. Previous studies have reported that C152 partitions primarily into the polar glycerol-backbone region of phosphatidylcholine (PC) bilayers, and that the partitioning behavior is strongly temperature dependent.[21–24]

The model biological membranes used are lipid vesicles comprised of 1,2-dipalmitoyl-*sn*-glycero-3-phosphocholine (DPPC) lipid vesicles. DPPC bilayers create diverse solvation environments across a distance of ∼4 nm consisting of (1) a nonpolar, hydrophobic region formed by DPPC's saturated, acyl tails; (2) a polar region arising from the lipids' ester groups and glycero-backbones; and (3) a zwitterionic phosphate head group (Figure 2). One point worth noting is that the environment created by DPPC's glycerol-backbone segment is polar but does not contain any explicit hydrogen bond donating groups.

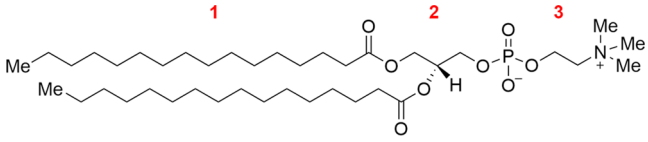

Figure 2. Chemical structure of 1,2-dipalmitoyl-*sn*-glycero-3-phosphocholine (DPPC) lipid. Number assignments correlate with various parts of lipid with the (1) hydrophobic hydrocarbon tail, (2) polar glycerol-backbone, and (3) zwitterionic phosphate head group.

Results presented here show that at ambient temperatures, approximately 60% of C152 partitions into the bilayer, with two-thirds of the partitioned solute molecules localized in the aprotic polar head group region and one-third solvated by the lipids' nonpolar acyl chains. Similarly, ∼60% of C151.5 partitions into the lipid bilayer with all of the partitioned solutes localized near the lipids' polar head groups. Contrary to predictions from the log *P* model, C151 shows no measurable partitioning into the lipid bilayer and remains solely in the aqueous buffer at all temperatures. Temperature-dependent changes in solute emission lifetimes suggest that the increase in C152 partitioning as the membrane passes through its gel–

https://dx.doi.org/10.1021/acs.jpcb.0c06109
J. Phys. Chem. B 2020, 124, 8299–8308

Scheme 1. Synthesis of C151.5

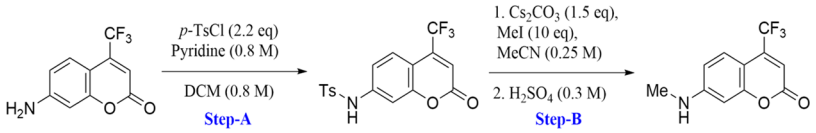

Table 1. Fluorescence Properties of C151, C151.5, and C152[e]

	C151					C151.5					C152				
solvent	λ_{exc} (nm)	λ_{em} (nm)	τ_f (ns)[a]	φ_f[b]	k_f[b] (10^7 s^{-1})	λ_{exc} (nm)	λ_{em} (nm)	τ_f (ns)[a]	φ_f[c]	k_f[c] (10^7 s^{-1})	λ_{exc} (nm)	λ_{em} (nm)	τ_f (ns)[a]	φ_f[d]	k_f[d] (10^7 s^{-1})
PBS buffer	336	490	4.51	0.01[c]	11.8	389	514	3.47	0.31	8.9	400	520	0.62(0.92) 4.15(0.08)	0.05	8.1
methanol	379	479	5.26	0.37[d]	11.11	388	503	4.50	0.76	16.9	396	509	1.03	0.09	8.3
acetonitrile	367	459	5.24	0.57[d]	6.97	381	488	5.49	0.28	5.1	392	494	2.07	0.22	9.8
cyclohexane	348	397	1.21(0.65) 3.27(0.35)	0.28[d]	23.37	356	436	4.03	0.45	11.2	373	426	4.39	0.97	25.1

[a]Lifetimes are ±0.2−0.3 ns. Numbers in parentheses next to lifetimes are amplitudes of that lifetime. [b]Quantum yields (ϕ_r) and radiative rates (k_r) reported by Pal et al. and Gobrogge et al.[21−24,31] [c]Quantum yields (ϕ_r) and radiative rates (k_r) measured in this work. [d]Quantum yields (ϕ_r) and radiative rates (k_r) reported by Pal et al.[32] [e]Fluorescence excitation and emission spectra for all three solutes in bulk solvents are shown in the supporting information (Figures SI-4−SI-6). How the quantum yields and radiative rates were calculated can be seen in the supporting information.

liquid crystalline transition is accompanied by water also moving into the bilayer's polar head group region. C151.5, however, shows no corresponding evidence of associating with the hydration of the bilayer at any temperature. Collectively, these results illustrate the limitations of using macroscopic descriptors to infer mechanistic details involving solute partitioning into biological membranes.

EXPERIMENTAL METHODS

Materials. Solvents were purchased from Sigma-Aldrich and used as received. Millipore water (18.2 MΩ) was used to make a phosphate-buffered saline. 1,2-Dipalmitoyl-*sn*-glycero-3-phsophocholine (16:0 DPPC) was purchased from Avanti Polar Lipids. Laser grade C151 and C152 were purchased from Exciton and used as received. C151.5 was synthesized according to the procedure shown in Scheme 1 with modification to ref 27. A more detailed description of the synthesis can be found in the Supporting Information (Figure SI-1). All bulk solvent solutions were made at 6 μM concentrations with 1.5 mM DPPC vesicles used for fluorescence experiments and 20 mM DPPC vesicles made for thermoanalytical experiments.

Lipid Bilayer Vesicle Preparation. Lipid bilayer vesicles were prepared by dissolving DPPC in chloroform. The solvent was then removed via rotary evaporation. The resulting thin lipid film was subsequently rehydrated using a 6 μM coumarin and 10 mM phosphate-buffered saline (PBS, pH = 7) to form a lipid vesicle solution. The solution was sonicated for 30 min at ∼50 °C. The solution was heated (50 °C) and passed through an Avanti Mini Extruder 10 times with a membrane pore size of 200 nm.[21−24]

Time-Correlated Single-Photon Counting (TCSPC). Fluorescence lifetimes were measured using a Ti:sapphire oscillator (Coherent Chameleon, 80 MHz, 85 fs pulse duration, 680−1040 nm wavelength range) coupled with an APE autotracker capable of frequency doubling the fundamental to select solute-specific excitation wavelengths. A Conoptics model 350-10 modulator was used to reduce the repetition rate to 4 MHz. Picoquant PicoHarp 300 and FluoTime 200 software were used for data collection. Samples were equilibrated at reported temperatures for 5 min using a Quantum Northwest TC125 control. A neutral density filter (80% transmission >455 nm) was placed after the sample to reduce scattering from the vesicles. Photon emission was collected at wavelengths specific to each solute in bulk solvent as well as a wavelength that overlapped all emission spectra in bulk solvents. The excitation wavelength chosen was unique to each solute in bulk solvent as well as one that overlapped all of the bulk solvents in the excitation spectra, which was then used to excite the solute in vesicle solution. The difference in excitation and emission wavelengths between the bulk solvent wavelengths used for C15X in vesicle solution did not change fluorescence lifetimes of that system. Additional details about this assembly can be found in refs 21, 23, 24, 28, 29.

Time-resolved emission data from vesicle-containing solutions are fit with a linear combination of independent lifetimes and amplitudes using fitting parameters for that are adjusted to minimize residuals and optimize χ^2. The resulting fluorescent lifetimes are then compared to lifetimes of the solute in different solvents chosen to mimic local solvation environments within the lipid bilayer. The fluorescence decay and amplitude expression is shown in eq 4, where A_i and τ_i are the amplitude and lifetime of the ith component, respectively.[30]

$$I(t) = \int_0^t \mathrm{IRF}(t') \sum_{i=1}^{n} A_i e^{-t-t'/\tau_i} \tag{4}$$

Each trace was fit independently, without any constraints, for the lifetimes or amplitudes. The typical χ^2 were from 0.9 to 1.10 when accounting for at most three lifetimes. Typically, uncertainties in lifetimes and amplitudes were 0.2 ns and 0.04, respectively. Reported data represent the averaged results from at least four and sometimes as many as six experiments with independently prepared, equivalent samples. There is an intrinsic uncertainty in the lifetimes reported of ±0.2 ns due to the TCSPC instrument response function; however, the data and error bars presented in this work are four to six trials averaged together with a standard deviation reported for the average of those trials. The average lifetimes and amplitudes and their respective standard deviations are reported for each

https://dx.doi.org/10.1021/acs.jpcb.0c06109
J. Phys. Chem. B 2020, 124, 8299−8308

specific temperature and only compared to their respective temperatures.

RESULTS

Using the methods described above, we have examined how the molecular structure of C15X affects partitioning into model biological membranes. Prior to analyzing solute partitioning into DPPC bilayers, we measured time-resolved emission data from the C15X solutes in various solvation environments, modeled with bulk solvents. The bulk solvents were chosen to mimic specific solvation environments created within lipid bilayers: data from C15X in PBS buffer was used to identify the response from solutes that remained in bulk solution; acetonitrile approximated the polar aprotic head group region created by DPPC's ester groups; methanol was chosen to characterize solute behavior in polar, protic environments; and the nonpolar membrane interior was approximated with cyclohexane. Excitation and emission wavelengths and fluorescence lifetimes of C151, C151.5, and C152 are reported in Table 1. Time-resolved emission traces from all three solutes in bulk solvents are shown in Figure 3. Steady-state spectra for C15X in the bulk solvents are shown in the Supporting Information (Figures SI-4−SI-6). For the commercially available C151 and C152, data in Table 1 agree with previously reported findings in the literature.[29,31,32]

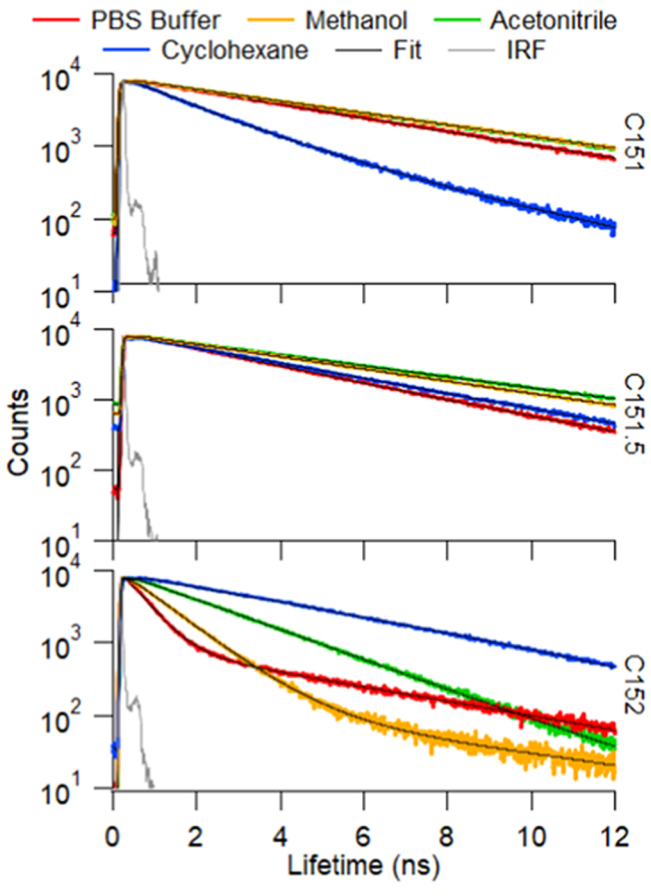

Figure 3. TCSPC spectra of 6 μM coumarins in bulk solvents taken at 10 °C. Top panel shows data for C151; the middle panel shows data for C151.5 and the bottom panel shows data for C152. Results from fitting these emission traces to eq 4 are reported in Table 1. Gray trace is instrument response function (IRF).

Both C151 and C152 show strong solvatochromic responses in their steady-state emission spectra consistent with an excited state having charge transfer character. (See the Supporting Information, Figures SI-4−SI-6.) Where C151 and C152 differ, however, is in their respective time-dependent emission properties in bulk solvents. In polar solvents, C151's time-resolved emission is characterized by a single exponential decay having relatively long lifetimes that depend on proticity. In the PBS buffer, C151's emission lifetime is 4.51 ns; in both methanol and acetonitrile, the emission lifetime lengthens to 5.25 ns. In a nonpolar solvent (cyclohexane), the dominant contribution to a biexponential decay is considerably shorter (1.21 ns). C151's solvent-dependent emission behavior has been attributed photoisomerization, where excited state C151 can form a planar intramolecular charge transfer (ICT) state that is stabilized in polar media.[29,31,32] In contrast to C151, C152 is believed to form a nonradiative, twisted intramolecular charge transfer (TICT) state in polar, protic environments with a correspondingly short, sub-ns emission lifetime.[31−33] In nonpolar solvents that do not enable the nonradiative decay pathway, C152's lifetime lengthens to 4.39 ns. Solute emission lifetimes are largely independent of temperature over the 10−70 °C window used in this work, with lifetimes changing by ≤0.4 ns between the two extremes.

C151.5's photophysical properties are being reported for the first time, we note that C151.5's steady-state emission red-shifts almost 80 nm as solvent polarity changes from a nonpolar limit (cyclohexane) to an aqueous environment (Figures SI-4−SI-6). This large bathochromic shift implies that C151.5's first excited state—like those of C151 and C152—also has a degree of charge transfer character. From the perspective of using C151.5 as an intermediate for testing membrane partitioning and the accuracy of log P as a partitioning predictor, C151.5's time-dependent emission behavior shows measurable differences between C151.5 in the different bulk solvents with ∼0.5 ns differences between the PBS buffer (3.47 ns), cyclohexane (4.03 ns), methanol (4.50 ns), and acetonitrile (5.49 ns).

Using ChemDraw Prime 19.0, we calculated log P values for C151 (1.6), C151.5 (1.9), and C152 (2.7). ChemDraw Prime uses a summation of the lipophilicity of each of the molecule's functional groups to calculate the log P value. We note again that all C15X solutes meet the Lipinski Ro5 criteria and should be suitable candidates for bioconcentration in lipid membranes with C152 (log P = 2.7) having the highest affinity and C151 (log P = 1.6) the lowest. The log P value predicts that C151.5 (log P = 1.9) should behave more like C151 than C152.

Figure 4 shows the temperature-dependent time-resolved emission from all three C15X solutes in solutions containing DPPC vesicles. As noted in the Experimental Methods section, each decay was fit using eq 4 and the resulting lifetime and amplitude data are reported in Table 2. For all emission traces, the minimum number of lifetimes were included that could adequately describe the data as determined from the resulting residuals and χ^2 values. Data for selected temperatures are reported in Table 2, and Figure 5 summarizes the lifetime results for all three solutes in DPPC vesicle solutions measured as a function of temperature. A full collection of lifetimes and amplitudes is provided in the Supporting Information (Table SI-1). An important point to note is that no effort is made to constrain the C15X calculated lifetimes in vesicle solutions to those measured in the bulk solvents. Rather, C15X lifetimes in vesicle solutions were first calculated and then compared to

https://dx.doi.org/10.1021/acs.jpcb.0c06109
J. Phys. Chem. B 2020, 124, 8299−8308

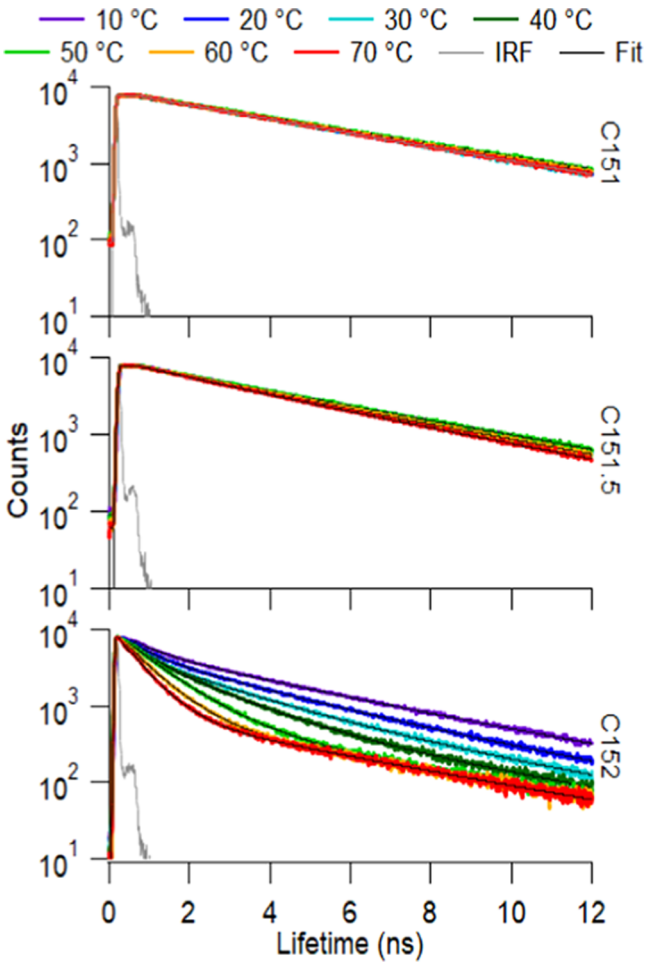

Figure 4. TCSPC spectra of Coumarins in DPPC as a function of temperature. Top panel shows data for C151; the middle panel shows data for C151.5 and the bottom panel shows data for C152. Results from fitting these emission traces to eq 4 are reported in Table 3.

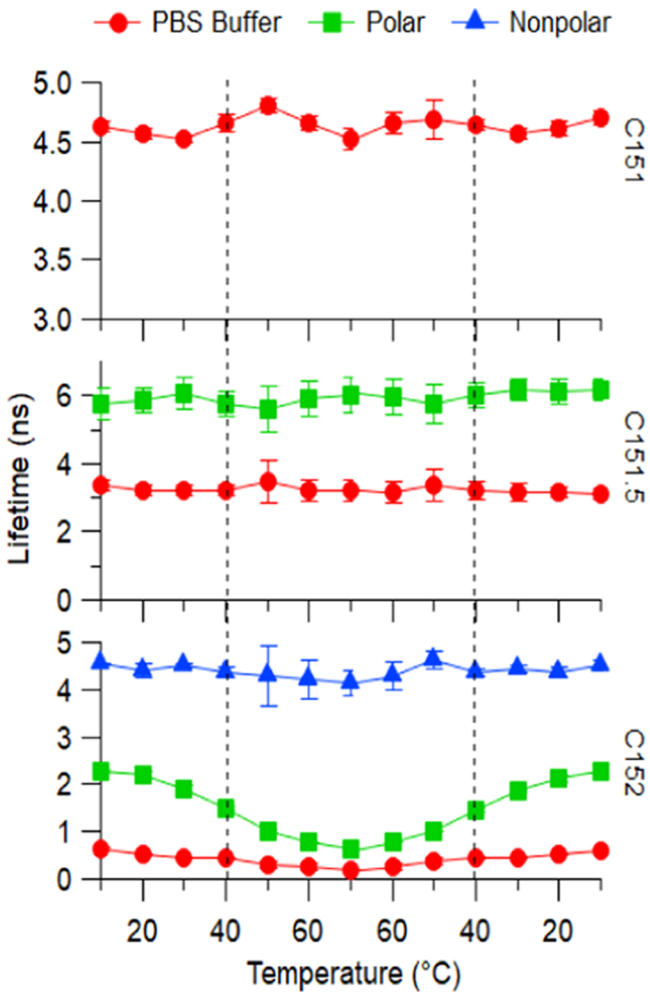

Figure 5. Fluorescence lifetimes of C15X in DPPC with three potential partitioning environments: PBS buffer (τ_1, red circles), polar head group (τ_2, green squares), and nonpolar tails (τ_3, blue triangles). The dashed lines represent DPPC transition temperature from gel to liquid-crystalline state at 41 °C. Error bars on each point reflect the one standard deviation uncertainty of several (4−6) measurements averaged together. In some cases, the uncertainty is smaller than the symbols used to represent the data.

bulk solvent lifetimes to determine the nature of the local solvation environment the solutes experiences and if/when they were absorbed by the bilayer. Furthermore, even though data shown in Figure 4 were acquired using single excitation and emission wavelengths, these wavelengths were chosen so that they overlapped with excitation and emission spectra of the C15X solutes in all four model solvents. Control experiments demonstrated that in the model solvents, emission lifetimes did not change from those reported in Table 1 (acquired at different wavelengths) and those measured with the common excitation wavelength. (Data not shown.)

Several observations about the data in Figure 4 and Table 2 stand out. First, fluorescence emission trends of C15X differ

Table 2. Selected Fluorescence Lifetimes (in ns) and Amplitudes (in Parentheses) of Coumarins in DPPC at a Temperature Ramp from 10, 30, 50, and 70 °C and Back Down to 10 °C

	C151	C151.5		C152		
temp. (°C)	buffer τ_1	buffer τ_1 (A_1)	polar τ_2 (A_2)	buffer τ_1 (A_1)	polar τ_2 (A_2)	nonpolar τ_3 (A_3)
10	4.62	3.37 (0.34)	5.73 (0.66)	0.62 (0.43)	2.27 (0.39)	4.55 (0.18)
30	4.52	3.22 (0.48)	6.09 (0.52)	0.45 (0.47)	1.99 (0.49)	4.56 (0.04)
50	4.81	3.48 (0.29)	5.59 (0.71)	0.35 (0.10)	1.03 (0.88)	4.61 (0.02)
70	4.52	3.19 (0.54)	6.03 (0.46)	0.32 (0.20)	0.65 (0.78)	4.25 (0.02)
50	4.69	3.36 (0.29)	5.74 (0.71)	0.39 (0.11)	1.03 (0.87)	4.73 (0.02)
30	4.57	3.18 (0.39)	6.16 (0.61)	0.43 (0.42)	1.88 (0.53)	4.41 (0.05)
10	4.70	3.09 (0.30)	6.15 (0.70)	0.65 (0.43)	2.34 (0.38)	4.56 (0.19)

[a]Amplitudes have been corrected for their respective radiative rates (see text). Uncertainties in lifetimes are ±0.2 ns; uncertainties in amplitudes are ±0.04.

https://dx.doi.org/10.1021/acs.jpcb.0c06109
J. Phys. Chem. B 2020, 124, 8299−8308

significantly as a function of temperature. While emission lifetime from C151 does not change as the vesicle solution temperature is cycled from 10 to 70 °C and back down, C152 emission changes markedly. C151.5 time-resolved emission lifetimes show small but measurable changes as a function of temperature. C151 emission can be fit with a single lifetime of ~4.6 ns, a result that is indistinguishable from C151 emission in pure PBS buffer. On this basis, we conclude that C151 does not partition into the DPPC vesicle bilayers, despite its favorable structural properties and log *P* value.

Fitting C152's time-resolved emission requires a minimum of three exponential decays: a long decay corresponding to a fluorescence lifetime ≥4 ns, a short, sub-ns lifetime, and an intermediate lifetime that changes reversibly from 2.2 ns at 10 °C to 0.6 ns at 70 °C. Similar to C152's 4.4 ns lifetime in cyclohexane, the longer lifetime is assigned to C152 in the nonpolar environment created by DPPC's acyl chains. These results match previously reported findings.[21−24] The short lifetime matches C152's behavior in PBS buffer. The intermediate lifetime changes from a polar aprotic limit (2.2 ns) to a polar protic limit (≤1ns) as the solution passes through its gel−liquid crystalline transition temperature (T_{gel-lc}) at 41 °C. This behavior has been observed previously and has been interpreted as evidence of water intercalation into the polar region of the lipid bilayer as the bilayer melts.[21] The relevance of this shift in fluorescence lifetime corresponding to the lipids phase transition for solute partitioning is discussed in more detail below.

C151.5's time-resolved emission is characterized by two fluorescent lifetimes: a short lifetime of ~3.3 ns that is assigned to C151.5 in the PBS buffer and a longer lifetime of 5.9 ns that is longer than emission in any bulk solvent, but most closely matches C151.5 emission in a polar, aprotic environment (5.5 ns). The population of C151.5 responsible for this long-lived emission is assigned to C151.5 that has partitioned into the lipid bilayer's polar head group and glycerol-backbone regions. Unlike C152, this long C151.5 lifetime does not show evidence of transitioning to a value consistent with polar, protic solvation as the bilayer passes through T_{gel-lc}. As discussed below, we believe that these observations provide important details about the mechanisms responsible for C152 and C151.5 partitioning into DPPC membranes.

Data in Figure 4 can be used to determine quantitative populations of solutes partitioning into DPPC membranes after the amplitudes have been corrected for their respective radiative rates.[22] To do this, we used radiative rates for C152 in the bulk solvents that most closely approximated the corresponding lifetimes that were used (Amplitude data in Table 2 are radiative rate corrected and correspond to the solute population within the membrane). C151's radiative rate in water has been reported previously and was confirmed in our own laboratory. C151.5's quantum yields and radiative rates in various solvents are reported here for the first time. Radiative rate corrected amplitudes from the time-resolved emission data in Figure 4 are shown in Figure 6.

While C152 and C151.5 show changes to their respective fluorescence decay's as a function of temperature, C151 shows no change in its fluorescence lifetimes and is assumed to remain completely in the aqueous solution. As reported previously, C152 shows strong uptake by the bilayer in the vicinity of the gel−liquid crystalline transition temperature (41 °C) with up to 90% of the available solute molecules absorbed into the bilayer.[22] Based on lifetime amplitudes, above the

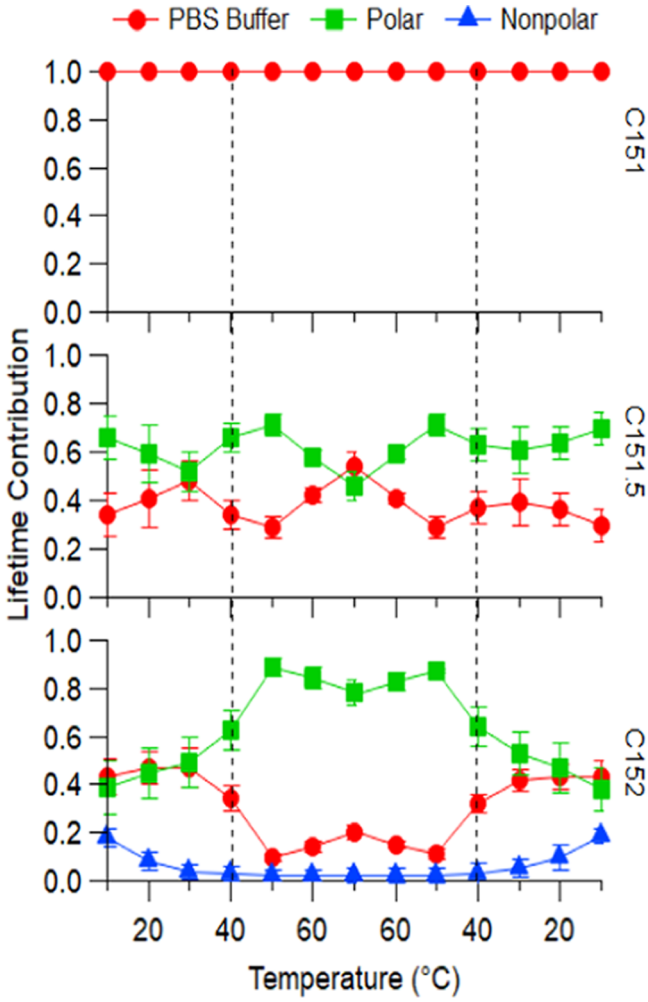

Figure 6. Radiative rate corrected fluorescence contribution of C15X in DPPC with three potential contribution environments: PBS buffer (τ_1, red circles), polar head group (τ_2, green squares), and nonpolar tails (τ_3, blue triangles). The dashed lines represent DPPC transition temperature from gel to liquid-crystalline state at 41 °C. Error bars on each point reflect the uncertainty of several measurements averaged together.

T_{gel-lc}, C152 exsolvates out of the aqueous buffer and the nonpolar region of the bilayer into the polar head group where 88% of C152 is localized. This behavior is reversible as the temperature is cycled above and below the T_{gel-lc}.

Despite having structural similarities and a similar log P value to C151, C151.5 shows behavior more similar to that of C152. Specifically, the biexponential decay of C151.5 in DPPC implies that C151.5 has some affinity for the DPPC membrane and the radiative rate adjusted amplitudes show that up to 70% of the C151.5 is solvated in a polar, aprotic environment near the transition temperature. Above the transition temperature, partitioning appears to be enthalpically unfavorable as further increases in temperature drive a small amount of exsolvation from the bilayer back into the aqueous solution. However, C151.5 does not show the same dramatic uptake by the DPPC bilayer in the vicinity of the transition temperature, nor does C151.5 ever show any affinity for the nonpolar lipid bilayer interior. C151.5's amplitudes suggest more nuanced partitioning behavior below the transition temperature (with evidence for small amounts of exsolvation below 41 °C), but interpreting these observations would require additional

https://dx.doi.org/10.1021/acs.jpcb.0c06109
J. Phys. Chem. B 2020, 124, 8299−8308

experiments with finer temperature resolution between 10 and 40 °C.

Given the markedly different affinities C15X solutes appear to have for DPPC bilayers, we performed differential scanning calorimetry (DSC) measurements determine if solute partitioning affected the gel−liquid crystalline melting temperature of pure DPPC bilayers. DSC traces shown in Figure 7 illustrate

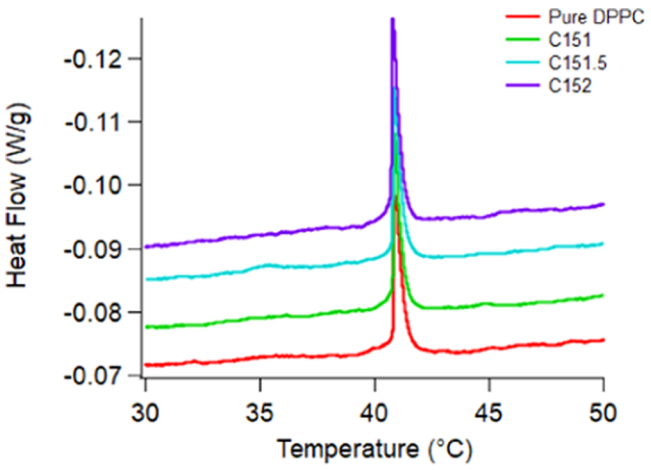

Figure 7. DSC spectra of pure DPPC vesicle solutions and DPPC vesicle solutions containing 6 μM C151, C151.5 or C152. All transitions are endothermic and offset for ease of viewing.

that DPPC's T_{gel-lc} remains unchanged by partitioning of coumarin solutes, even C152. This result is surprising given the strong uptake of C152 into the bilayer near the transition temperature. DSC traces of DPPC vesicle-containing solutions with C151.5 also show no difference from data acquired with pure DPPC vesicle solutions.

DISCUSSION

Given the findings shown in Figure 5 and 6 and reported in Table 2, two phenomena require explanation:

- Differences in C15X uptake by the lipid bilayer as a function of solute identity and temperature
- The role of water in C15X/DPPC bilayers solvation.

The discussion below considers each phenomenon, focusing on changes in DPPC vesicle bilayer structure as it melts and the noncovalent associations that are involved as well as the membrane hydration as a function of the bilayer phase.

Differences in C15X Uptake. Solute transfer between two adjacent (liquid) phases is often analyzed in the context of a Flory−Huggins model that considers the volume changes required for a solute to migrate from one medium into the other (eq 5).[34,35]

$$\Delta(\Delta G)_{FH} = -RT \ln\left(\frac{[x]_{org}}{[x]_{aq}}\right) - RT\left(\frac{V_x}{V_{aq}} - \frac{V_x}{V_{org}}\right) \quad (5)$$

Here, $\Delta(\Delta G)_{FH}$ is a Flory−Huggins-based description of the solvation energy change when a solute migrates between phases, $[x]_i$ is the concentration of the solute in the organic and aqueous phases, and V_i are the molar volumes of the solute, water, and organic medium. Given that $V_{C152} > V_{C151.5} > V_{C151}$ and that $V_{aq} < V_{org}$ (where V_{org} for DPPC will correspond that part of the organic structure that must be rearranged to accommodate an incoming solute), eq 5 predicts that C152 partitioning into the bilayer should make the largest favorable (=negative) contribution to the system's overall free energy. This same size-only consideration predicts that C151 partitioning will have the smallest impact on $\Delta(\Delta G)_{FH}$. C151.5's contribution to $\Delta(\Delta G)_{FH}$ will be intermediate between the C152 and C151. Qualitatively this description captures differences in C15X partitioning at temperatures above T_{gel-lc}.

This Flory−Huggins description, however, cannot account for all of the observed partitioning behaviors. At the lowest temperatures sampled in this work (10 °C), ∼20% more C151.5, compared to C152, partitions into the bilayer (Table 2). The amount of C151.5 in the bilayer changes little as a function of temperature, varying between ∼70 (50 °C) and ∼50% (70 °C). Across most of the temperature range sampled, the amount of C151.5 in the bilayer fluctuates between ∼55 and 60%. In contrast, C152 partitioning shows a strong temperature dependence with ∼90% of the available solute taken up by the membrane at 50 °C and ∼55% at 10 °C.

Previous descriptions of C152 partitioning into DPPC lipid bilayers have included a van't Hoff analysis and noted that C152 partitioning showed several temperature discontinuities.[21] Above T_{gel-lc}, C152 partitioning was exothermic ($\Delta H_{partitioning}$ = −48 kJ/mol) and entropically unfavorable ($\Delta S_{partitioning}$= −133 J/(mol K)). At temperatures well below the melting transition, C152 partitioning was weakly exothermic ($\Delta H_{partitioning}$ = −8 kJ/mol) and, again, entropically unfavorable ($\Delta S_{partitioning}$= −26 J/(mol K)). Between 30 and 40 °C, however, C152 partitioning became endothermic ($\Delta H_{partitioning}$ = +85 kJ/mol) and entropically favorable ($\Delta S_{partitioning}$= 278 J/(mol K)).[21] These quantitative enthalpic and entropic changes between 30 and 40 °C coincide with the temperature window where DPPC bilayers exist in a metastable "ripple" phase characterized by domains of a splayed gel phase and a crystalline, interdigitated gel phase separated by regions of disordered lipids.[36]

A similar van't Hoff analysis has been performed with the C151.5 partitioning data (Supporting Information, Figure SI-8. Data for C152 are included for comparative purposes in Figure SI-9). In the pretransition temperatures (T_{pre}), below T_{gel-lc}, the thermodynamic quantities associated with C151.5 partitioning show striking differences from those of C152. Specifically, from the lowest temperature sampled in this work 10−40 °C, C151.5 partitioning shows virtually no thermal dependence ($\Delta H_{partitioning}$ = −2.5 ± 2 kJ/mol; $\Delta S_{partitioning}$ = −3.2 J/(mol K)). Above the transition temperature, C151.5 partitioning shows a similar dependence to C152, but with slightly attenuated enthalpic and entropic contributions. ($\Delta H_{partitioning}$ = −48 kJ/mol; $\Delta S_{partitioning}$ = −142 J/(mol K)). Results from the van't Hoff analyses for both solutes are reported in Table 3.

These differences between C151.5 and C152, especially below T_{gel-lc}, are striking and suggest that their partitioning behaviors are driven by fundamentally different mechanisms. C151.5 partitioning is largely insensitive to the bilayer phase and system temperature, whereas bilayer disorder significantly enhances C152 partitioning. Again, we note that C151 shows no measurable tendency to associate with the bilayer at any temperature. The sole structural differences between the three solutes occur at the 7-amine position. All three solutes can accept hydrogen bonds through the amine's lone pair (as well as each solute's ester group), but C152 cannot donate

https://dx.doi.org/10.1021/acs.jpcb.0c06109
J. Phys. Chem. B 2020, 124, 8299−8308

Table 3. Results from a van't Hoff Analysis of C151.5's Temperature-Dependent Partitioning Behavior[a]

		C151.5	C152
ΔH (kJ/mol)	$T < T_{pre}$	−2.5	−8
	$T_{pre} \leq T \leq T_{gel-lc}$		85
	$T > T_{gel-lc}$	−48	−48
ΔS (J/(mol K))	$T < T_{pre}$	−3.2	−26
	$T_{pre} \leq T \leq T_{gel-lc}$		278
	$T > T_{gel-l-c}$	−142	−133

[a](See Figure SI-8). Uncertainties in reported enthalpies are ≤4 kJ/mol, and uncertainties in reported entropies are ≤10 J/(mol K). Values reported for C152 are included for comparative purposes and were taken from ref 21 (see Supporting Information Figure SI-9). Note that the signs of ΔH and ΔS assume that $C15X_{aq}$ is the "reactant" and $C15X_{membrane}$ is the "product".

hydrogen bonds, whereas C151 and C151.5 can donate 2 and 1 hydrogen bonds, respectively.

In light of the C15X behaviors shown in Figure 6 and Table 3, we propose that C151's ability to form strong hydrogen bonds with the aqueous buffer prevents it from partitioning into the bilayer, despite a favorable log P value of 1.6. Below T_{gel-lc} and in the T_{pre}, DPPC vesicles are irregularly shaped and adopt "crumpled" structures with complex, irregularly shaped topological defects.[37] Similarities in the C151.5 and C152 behavior at lower temperatures imply that noncovalent association is driving both species to partition into the bilayer—presumably through defects in the well-ordered, frozen bilayer membrane structure—with those solutes in the polar head group region being solvated in an aprotic environment. Compared to C151.5, a larger fraction of the more hydrophobic C152 partitions into the hydrophobic region created by the acyl chains. As the membrane begins to melt (at the pretransition), the disordered region(s) of the bilayer can accommodate more C152, albeit at an enthalpic cost of +85 kJ/mol. Driving this partitioning, however, is an accompanying increase in system entropy that results from removing the hydrophobic solute from its aqueous solvation cavity. From a molecular perspective, C152 partitioning can be enhanced by the large lateral density fluctuations reduction that accompany the formation of DPPC's disordered phase.[38,39] Data reported in Table 3 show clearly that C151.5 is not sensitive to the bilayer structure below T_{gel-lc}. Above T_{gel-lc} both C152 and C151.5 show similar partitioning behaviors with solute exsolvation from the bilayer being driven by a large, exothermic contribution. The negative change in partitioning entropy above T_{gel-lc} for both solutes is interpreted as a loss of entropy in the buffer as the solvent needs to accommodate the relatively hydrophobic solutes.

Water's Role in Solute Partitioning. The second observation from the C15X partitioning data requiring discussion is apparent in Figure 5: C152's polar head group solvation lifetime shortens from 2.3 ns at low temperatures to ≤1.0 ns at higher temperatures. This change implies that C152 solvation in the polar head group region changes from a polar, aprotic environment to a polar, protic environment as the DPPC bilayer melts. In contrast, C151.5's polar head group solvation lifetime remains relatively constant at 5.9 ± 0.2 ns across the entire temperature range sampled. As noted in the results section, this value most closely matches C151.5 solvated in a polar, aprotic environment (τ = 5.5 ns in acetonitrile) and is far from the C151.5 emission lifetime in polar, protic media (τ = 4.5 ns in methanol; 3.5 ns in aqueous buffer).

Studies have shown that water content in a lipid bilayer increases when the bilayer transitions from its gel to liquid-crystalline state.[40−43] As a DPPC bilayer passes from its well-ordered gel state to disordered liquid crystalline, the membrane swells and the average area per lipid molecule increases from 57 to 65 Å^2/lipid.[44−46] Pandey et al. used classical molecular dynamics simulations to predict that in the expanded state, the choline's cationic $N(CH_3)_3^+$ group folds toward the membrane, bringing with it noncovalently bound water molecules.[47] This same study predicted that above the transition temperature, water molecules could be found throughout the nonpolar tails albeit with decreasing concentration. Similarly, Alarcon, et al. calculated that the amount of water in the bilayer doubled as the bilayer passed from its gel to liquid-crystalline state.[40] This prediction from classical MD simulations was verified by Umakoshi and co-workers who used time-resolved emission spectra from the probe Laurdan to create "water maps" and estimate water population per lipid.[43] Water in the bilayer tends to be organized in string or branched structures having lower H-bond coordination with only a small population of isolated monomers.[40]

We propose that C152 solvation in DPPC bilayers is sensitive to bilayer hydration, while C151.5 solvation in the bilayer is not. From this difference, we infer that C152 solvated in the polar head group region is not as strongly associated through noncovalent interactions with the polar head group as is C151.5. If this supposition is true, C152 will be able to utilize the increased water concentration in the bilayer that accompanies melting to accept a hydrogen bond through C152's amine lone pair. In contrast, if C151.5's noncovalent interactions in the polar head group region—most notably hydrogen bonds to either the choline or ester groups—are suitably strong and prevent partitioned solutes from interacting with water molecules already in the (gel-phase) bilayer, then we surmise C151.5 will be insensitive to the influx of additional water following melting. While this interpretation is admittedly speculative and does not explicitly consider the specific contributions from water entering the bilayer, it does raise interesting questions about the role water plays in facilitating bioconcentration and intramembrane chemistry.

CONCLUSIONS

Understanding a solute's tendency for bioconcentration is a topic of interest as it could lead to adverse ecological or physiological effects and require a costly remediation in the future. This work examined how three closely related 7-aminocoumarin solutes partitioned into DPPC lipid bilayers as a function of temperature. All three solutes have log P values that predict strong membrane affinity; however, each solute exhibited distinctively different partitioning behavior. C151 with a log P value of 1.6 showed no partitioning into the DPPC bilayer regardless of temperature and lipid bilayer phase. C151.5 has a log P value of 1.9 partitioned only into the bilayer's polar head group region, and the amount of C151.5 that partitioned into the bilayer varied only slightly with temperature and lipid bilayer phase. C152 partitioning showed a strong temperature dependence with ∼90% of the available solute being absorbed into the bilayer near the DPPC transition temperature, qualitatively consistent with a log P value of 2.5.

https://dx.doi.org/10.1021/acs.jpcb.0c06109
J. Phys. Chem. B 2020, 124, 8299−8308

These differences illustrate clearly that membrane partitioning and the tendency of a solute to bioconcentrate depends on more than simply differential solubilities between aqueous and polar organic (e.g., 1-octanol) phases. In predicting bioconcentration, additional factors must be considered, including specific solvation forces such as solute-hydrogen bonding. The data suggest differences in partitioning mechanisms that provide clear benchmarks for further experimental and computational studies.

■ ASSOCIATED CONTENT

Supporting Information

The Supporting Information is available free of charge at https://pubs.acs.org/doi/10.1021/acs.jpcb.0c06109.

Synthesis procedures of C151.5 as well as the H NMR and ^{13}C NMR of the final product; full steady-state excitation and emission spectra of C15X in each of the bulk solvents and the bathochromic properties are seen in the emission spectra of C15X; full collection of lifetimes and amplitudes of C15X in DPPC as a function of temperature; fluorescence decay traces of C151 and C151.5 in DPPC; figures used for the van't Hoff analysis of C151.5 and C152 (PDF)

■ AUTHOR INFORMATION

Corresponding Author

Robert A. Walker − *Department of Chemistry and Biochemistry and Montana Materials Science Program, Montana State University, Bozeman, Montana 59717, United States;* orcid.org/0000-0002-0754-6298; Phone: 406-994-7928; Email: rawalker@montana.edu

Authors

Katelyn M. Duncan − *Department of Chemistry and Biochemistry, Montana State University, Bozeman, Montana 59717, United States*

Aoife Casey − *Department of Chemistry and Biochemistry, Montana State University, Bozeman, Montana 59717, United States*

Christine A. Gobrogge − *Department of Chemistry and Biochemistry, Montana State University, Bozeman, Montana 59717, United States*

Rhys C. Trousdale − *Department of Chemistry and Biochemistry, Montana State University, Bozeman, Montana 59717, United States*

Stefan M. Piontek − *Department of Chemistry and Biochemistry, Montana State University, Bozeman, Montana 59717, United States*

Matthew J. Cook − *Department of Chemistry and Biochemistry, Montana State University, Bozeman, Montana 59717, United States*

William H. Steel − *Department of Chemistry, York College of Pennsylvania, York, Pennsylvania 17403, United States*

Complete contact information is available at: https://pubs.acs.org/10.1021/acs.jpcb.0c06109

Author Contributions

The manuscript was written through the contributions of all authors. All authors have given approval to the final version of the manuscript.

Funding

This material is based upon the work supported in part by the National Science Foundation EPSCoR Cooperative Agreement OIA-1757351. Any opinions, findings, and conclusions or recommendations expressed in this material are those of the author(s) and do not necessarily reflect the views of the National Science Foundation.

Notes

The authors declare no competing financial interest.

■ ACKNOWLEDGMENTS

W.H.S. gratefully acknowledges sabbatical support from York College (PA).

■ REFERENCES

(1) Linde, C. D. *Physico-Chemical Properties and Environmental Fate of Pesticides*; State of California Environmental Protection Agency: Sacramento, California, 1994; pp 1−53.

(2) Lipinski, C. A. Drug-like properties and the causes of poor solubility and poor permiability. *J. Pharmacol. Toxicol. Methods* **2000**, *44*, 235−249.

(3) Neely, W. B. B.; Gary, E. *Environmental Exposure From Chemicals*; CRC Press: Boca Raton, FL, 2018; Vol. *1*, p 254.

(4) Neely, W. B. B.; Gary, E. *Environmental Exposure from Chemicals*; CRC Press: Boca Raton, FL, 2018; Vol. *2*, p 159.

(5) Pollastri, M. P. Overview on the Rule of Five. *Curr. Protoc. Pharmacol.* **2010**, *49*, 9.12.1−9.12.8.

(6) Verber, D. F.; Johnson, S. R.; Cheng, H.-Y.; Smith, B. R.; Ward, K. W.; Kopple, K. D. Molecular Porperties tha tINfluence the Oral Bioavailability of Drug Candidates. *J. Med. Chem.* **2002**, *45*, 2615−2623.

(7) Calamari, D. Assessment of persistent and bioaccumulating chemicals in the aquatic environment. *Toxicology* **2002**, *181−182*, 183−186.

(8) Rodrigues, E. T.; Alpendurada, M. F.; Ramos, F.; Pardal, M. A. Environmental and human health risk indicators for agricultural pesticides in estuaries. *Ecotoxicol. Environ. Saf.* **2018**, *150*, 224−231.

(9) Sim, M. Case studies in the use of toxicological measures in epidemiological studies. *Toxicology* **2002**, *181−182*, 405−409.

(10) Arnot, J. A.; Gobas, F. A. P. C. A review of bioconcentration factor (BCF) and bioaccumulation factor (BAF) assessments for organic chemicals in aquatic organisms. *Environ. Rev.* **2006**, *14*, 257−297.

(11) Nichols, J. W.; Mark, B.; Dimitrov, S. D.; Escher, B. I.; Han, X.; Kamert, N. Bioaccumulation Assesment Using Predictive Approaches. *Integr. Environ. Assess. Manage.* **2009**, *5*, 577−597.

(12) Steel, W. H.; Foresman, J. B.; Burden, D. K.; Lau, Y. Y.; Walker, R. A. Solvation of nitrophenol isomers: consequences for solute electronic structure and alkane/water partitioning. *J. Phys. Chem. B* **2009**, *113*, 759−766.

(13) Hoffman, D. J. R.; Barnett, A.; Burton, G. A., Jr.; Cairns, J., Jr. *Handbook of Ecotoxicology*, 2nd ed.; Lewis Publishers: Boca Raton, 2003.

(14) Chiou, C. T. F.; Virgil, H.; Schmedding, D. W.; Kohnert, R. L. Partition Coeffcient and Bioaccumulation of Selected Organic Chemicals. *Environ. Sci. Technol.* **1977**, *11*, 475−478.

(15) Chamberlain, K. E.; Avis, A.; Bromilow; Richard, H. 1-Octanol/Water Partition Coefficient (K_{ow}) and pK_a for Ionisable Pesticides Measured by a pH-Metric Method. *Pestic. Sci.* **1996**, *47*, 265−271.

(16) Leo, A.; Hansch, C.; Elkins, D. Partition coefficients and their uses. *Chem. Rev.* **1971**, *71*, 525−616.

(17) Lipinski, C. A.; Lombardo, F.; Dominy, B. W.; Feeney, P. J. Experimental and computational approaches to estimate solubility and permeability in drug discovery and development settings. *Adv. Drug Delivery Rev.* **2001**, *46*, 3−26.

(18) Steel, W. H.; Walker, R. A. Measuring dipolar width across liquid-liquid interfaces with 'molecular rulers'. *Nature* **2003**, *424*, 296−299.
(19) Valkó, K. Application of high-performance liquid chromatography based measurements of lipophilicity to model biological distribution. *J. Chromatogr. A* **2004**, *1037*, 299−310.
(20) Hughes, L. D. P.; David, S.; Nigsch, F.; Mitchell, J. B. O. Why Are Some Properites More Difficult to Predict than Others? A Study of QSPR Models of Solublility, Melting Point, and Log P. *J. Chem. Inf. Model.* **2008**, *48*, 220−232.
(21) Gobrogge, C. A.; Blanchard, H. S.; Walker, R. A. Temperature-Dependent Partitioning of Coumarin 152 in Phosphatidylcholine Lipid Bilayers. *J. Phys. Chem. B* **2017**, *121*, 4061−4070.
(22) Gobrogge, C. A.; Kong, V. A.; Walker, R. A. Temperature Dependent Solvation and Partitioning of Coumarin 152 in Phospholipid Membranes. *J. Phys. Chem. B* **2016**, *120*, 1805−1812.
(23) Gobrogge, C. A.; Kong, V. A.; Walker, R. A. Temperature-Dependent Partitioning of C152 in Binary Phosphatidylcholine Membranes and Mixed Phosphatidylcholine/Phosphatidylethanolamine Membranes. *J. Phys. Chem. B* **2017**, *121*, 7889−7898.
(24) Gobrogge, C. A.; Walker, R. A. Quantifying Solute Partitioning in Phosphatidylcholine Membranes. *Anal. Chem.* **2017**, *89*, 12587−12595.
(25) Moriguchi, I.; Hirono, S.; Nakagome, I.; Hirano, H. Compairson of Reliablitiy of log P Values for Drugs Calculated by Several Methods. *Chem. Pharm. Bull.* **1994**, *42*, 974−978.
(26) Xing, L. G.; Robert, C. Novel Methods for the Prediction of logP, pK_a, and logD. *J. Chem. Inf. Comput. Sci.* **2002**, *42*, 796−805.
(27) Li, J.; Zhang, C.-F.; Ming, Z.-Z.; Hao, G.-F.; Yang, W.-C.; Yang, G.-F. Coumarin-based novel fluorescent zinc ion probe in aqueous solution. *Tetrahedron* **2013**, *69*, 4743−4748.
(28) Purnell, G. E.; McNally, M. T.; Callis, P. R.; Walker, R. A. Buried Liquid Interfaces as a Form of Chemistry in Confinement: The Case of 4-Dimethylaminobenzonitrile at the Silica-Aqueous Interface. *J. Am. Chem. Soc.* **2020**, *142*, 2375−2385.
(29) Roy, D.; Liu, S.; Woods, B. L.; Siler, A. R.; Fourkas, J. T.; Weeks, J. D.; Walker, R. A. Nonpolar Adsorption at the Silica/Methanol Interface: Surface Mediated Polarity and Solvent Density across a Strongly Associating Solid/Liquid Boundary. *J. Phys. Chem. C* **2013**, *117*, 27052−27061.
(30) Becker, W. *Advanced Time-Correlated Single Photon Counting Techniques*; Springer: Berlin Heidelberg, Germeny, 2005; p 415.
(31) Nad, S. K.; Manoj; Pal, H. Photophysical Properties of Coumarin-152 and Coumarin-481 Dyes: Unusual Behavior in Nonpolar nad Higher Polarity Solvents. *J. Phys. Chem. A* **2003**, *107*, 4808−4816.
(32) Nad, S.; Pal, H. Unusual photophysical properties of coumarin-151. *J. Phys. Chem. A* **2001**, *105*, 1097−1106.
(33) Purnell, G. E.; Walker, R. A. Hindered Isomerization at the Silica/Aqueous Interface: Surface Polarity or Restricted Solvation? *Langmuir* **2018**, *34*, 9946−9949.
(34) Brem, R.; Chan, H. S.; Dill, K. A. Extracting microscopic energies from oil-phase solvation experiments. *J. Phys. Chem. B* **2000**, *104*, 7471−7482.
(35) Kumar, S. K.; Szleifer, I.; Sharp, K.; Rossky, P. J.; Friedman, R.; Honig, B. Size Dependence of Transfer Energies. 1. A Flory-Huggins Approach. *J. Phys. Chem. A.* **1995**, *99*, 8382−8391.
(36) De Vries, A. H.; Yefimov, S.; Mark, A. E.; Marrink, S. J. Molecuclar structure of the lecithin ripple phase. *Proc. Natl. Acad. Sci. U.S.A.* **2015**, *102*, 5392−5396.
(37) Hirst, L. S.; Ossowski, A.; Fraser, M.; Geng, J.; Selinger, J. V.; Selinger, R. L. Morphology transition in lipid vesicles due to in-plane order and topological defects. *Proc. Natl. Acad. Sci. U.S.A.* **2013**, *110*, 3242−3247.
(38) Jørgensen, K. I.; J, H.; Mouritsen, O. G.; Bennett, D.; Zuckermann, M. J. The effects of density fluctuations on the parititoning of foreign molecules into lipid bilayers: Application to anaesthetics and insecticides. *Biochim. Biophys. Acta, Biomembr.* **1991**, *1067*, 241−253.
(39) Mouritsen, O. G.; Zuckermann, M. J. Model of interfacial melting. *Phys. Rev. Lett.* **1987**, *58*, 389−392.
(40) Alarcón, L. M.; de Los Angeles Frias, M.; Morini, M. A.; Belen Sierra, M.; Appignanesi, G. A.; Anibal Disalvo, E. Water populations in restricted environments of lipid membrane interphases. *Eur. Phys. J. E* **2016**, *39*, No. 94.
(41) Foglia, F.; Lawrence, M. J.; Lorenz, C. D.; McLain, S. E. On the hydration of the phosphocholine headgroup in aqueous solution. *J. Chem. Phys.* **2010**, *133*, No. 145103.
(42) Pinto, O. A.; Disalvo, E. A. A new model for lipid monolayer and bilayers based on thermodynamics of irreversible processes. *PLoS One* **2019**, *14*, No. e0212269.
(43) Watanabe, N.; Suga, K.; Slotte, J. P.; Nyholm, T. K. M.; Umakoshi, H. Lipid-Surrounding Water Molecules Probed by Time-Resolved Emission Spectra of Laurdan. *Langmuir* **2019**, *35*, 6762−6770.
(44) Eze, M. O. Phase Tranistions in Phosopholipid Bilayers: Lateral Phase Separations Play Vital Roles in Biomembranes. *Biochem. Educ.* **1991**, *19*, 204−208.
(45) Leekumjorn, S.; Sum, A. K. Molecular studies of the gel to liquid-crystalline phase transition for fully hydrated DPPC and DPPE bilayers. *Biochim. Biophys. Acta, Biomembr.* **2007**, *1768*, 354−365.
(46) van Meer, G.; Voelker, D. R.; Feigenson, G. W. Membrane lipids: where they are and how they behave. *Nat. Rev. Mol. Cell Biol.* **2008**, *9*, 112−124.
(47) Pandey, P. R.; Roy, S. Headgroup mediated water insertion into the DPPC bilayer: a molecular dynamics study. *J. Phys. Chem. B* **2011**, *115*, 3155−3163.

https://dx.doi.org/10.1021/acs.jpcb.0c06109
J. Phys. Chem. B 2020, 124, 8299−8308